Improving the Temporal Resolution of Functional MR Imaging Using Keyhole Techniques

Jia-Hong Gao, Jinhu Xiong, Song Lai, E. Mark Haacke, Marty G. Woldorff, Jinqi Li, Peter T. Fox

Using a keyhole technique, it is shown that the data acquisition rate of gradient-echo imaging for functional MRI (fMRI) studies can be increased substantially. The resulting enhancement of the temporal resolution of fMRIs was accomplished without modifying the hardware of a conventional MRI system. High spatial resolution fMRI images were first collected with conventional full *k*-space acquisition and image reconstruction. Using the same data set, simulation reconstruction using the keyhole principle and zero-padding were performed for comparison with the full *k*-space reconstruction. No significant changes were found for fMRI images generated from the keyhole technique with a data sharing profile of 50% of the *k*-space. As *k*-space data sharing profiles increased to 75 and 87.5%, the keyhole fMRI images began to show only modest changes in activation intensity and area compared with the standard images. In contrast, zero-padding fMRI images produced a significant disparity both in activation intensity and area relative to the truly high-resolution fMRI images. The keyhole technique's ability to retain the intensity and area of fMRI information, while substantially reducing acquisition time, makes it a promising method for fMRI studies.

Key words: Functional MRI, keyhole, motor, temporal resolution.

INTRODUCTION

Intense interest has been aroused during the past few years in developing MRI techniques for studying human brain function (1). Most of these studies have used either echo-planar imaging (EPI) or conventional gradient-echo imaging pulse sequences. Although the conventional gradient-echo technique can be used to achieve better spatial resolution and is widely available compared with EPI, a major drawback is its relatively poor temporal resolution. In current functional MRI (fMRI) studies, the typical time resolution for a single slice is about 1 sec for the EPI technique and about 5–16 sec for conventional T_2*-weighted gradient-echo sequences. Higher temporal resolution is essential, not only for obtaining dynamic information about brain activity processes, but also in helping to reduce problems associated with subject motion artifacts. Although EPI has the higher temporal resolution necessary for these purposes, the hardware required to perform EPI is not widely available for most clinical MRI systems. Therefore, it is highly advantageous to develop techniques with improved temporal resolution based on conventional gradient-echo sequences.

The need for dynamic observation of tissue perfusion by imaging the passage of a contrast agent has motivated several groups to develop a fast imaging technique that is efficient and can be implemented in conventional MRI systems (2–4). This dynamic imaging technique, termed the keyhole technique, is based on the following principle: The central lines in *k*-space contribute primarily to the signal-to-noise ratio (SNR) and image contrast, whereas the peripheral lines in *k*-space contribute primarily to edge definition (5). In the keyhole technique, only the central fraction of the *k*-space data is collected, thereby increasing the temporal resolution of the dynamic images, while the missing peripheral lines in *k*-space data are supplied from reference images (i.e., data sharing). In this manner, an effective time resolution of about 1 sec per image can be achieved for T_2*-weighted gradient-echo schemes (6). The concept of data sharing has been previously discussed in conjunction with NMR fluoroscopy (5) and as a method for increasing the efficiency of fast spin-echo sequences (7, 8).

In this paper, we report the results of extending the keyhole technique to our fMRI studies. By applying this dynamic imaging technique, we can, in principle, improve the temporal resolution of gradient-echo imaging as much as four- or fivefold. This can yield a potential time resolution of 1 sec per image for the keyhole gradient-echo technique, thereby rendering it a useful alternative to EPI for studying the time course of brain activation. First attempts at applying the keyhole technique to fMRI studies have been presented by several groups (including ourselves) at recent MRI meetings (9–11). However, none of the abstracts presented in meetings have provided sufficient quantitation or analysis. To fully evaluate the value of the keyhole fMRI technique, a detailed description is necessary that includes statistical analysis of the keyhole fMRI images generated by different degrees of data sharing, along with direct comparison to conventional full *k*-space images. A comparison with zero-padding also needs to be performed to verify the value of filling peripheral *k*-space with shared values from the reference image rather than just with zeroes. Our comparison will focus on both activation area and activation intensity, as well as on the time course for the different analyses. This will be of general interest to the fMRI field and will help clinicians and neuroscientists become aware of the potential of keyhole fMRI, as well as

MRM 35:854–860 (1996)

From the Research Imaging Center, The University of Texas Health Science Center, San Antonio, Texas (J.-H.G., J.X., M.G.W., J.L., P.T.F.), and Mallinckrodt Institute of Radiology, Washington University School of Medicine, St. Louis, Missouri (S.L., E.M.H.).

Address correspondence to: Jia-Hong Gao, Ph.D., Research Imaging Center, The University of Texas Health Science Center at San Antonio, 7703 Floyd Curl Drive, San Antonio, TX 78284.

Received October 27, 1995; revised January 2, 1996; accepted January 2, 1996.

0740-3194/96 $3.00

its limitations, when applying this technique to clinical practice and neuroscience research.

METHODS

The principle of the keyhole technique is that each set of image acquisitions for a slice includes one "reference image" acquisition, which is a pulse sequence that completely fills the *k*-space (e.g., phase encoding, 256; frequency encoding, 256). The rest of the set consists of a series of limited *k*-space acquisitions in which only the central range (the "keyhole") of low-order phase encoding is repeatedly obtained. The high-order phase-encoded data from the reference acquisition in the set are combined with the low-order terms of each of the central *k*-space acquisitions in that set to complete the *k*-space for each of these data before a two-dimensional (2D) Fourier transform is performed. Because only the central *k*-space needs to be obtained for all the images in the set, except for the reference image, the image data can be acquired much more quickly than with conventional techniques.

To generate fMRI images, the *k*-space raw data are typically acquired during two brain states: an activation condition and a control condition (typically rest). An example of keyhole data acquisition for functional MRI is illustrated in Fig. 1, in which five images are acquired for each state. Each state has its own reference image; therefore, the between-condition differences in high-frequency information is in principle preserved in this keyhole fMRI data acquisition strategy. In our study, the middle image of each set was chosen as the reference image to minimize any potential imaging artifacts resulting from MRI system instability. As is typically done in fMRI, to enhance statistical power, the raw data were repeatedly acquired for several cycles (where each cycle includes a set of resting state images and a set of activation state images). A simple motor task (finger tapping) was used for activation, and the control condition was rest.

In the present study, we wanted to focus on the viability of the keyhole approach to obtain fMRI information compared with the conventional full *k*-space approach. Therefore, to eliminate other sources of variability as much as possible, including any variability of task performance or state, we analyzed the same data acquired from the subjects in a single session. To do this, we collected three cycles of off-on data from each subject, with each of the image samples acquired as a conventional full *k*-space sweep. These data were then reconstructed and analyzed in three different ways:

- The conventional way—using all of the *k*-space data from each of the acquisitions.
- An analytical simulation of the keyhole approach (Fig. 1)—in which, for each series of five image acquisitions for each state half-cycle, the middle acquisition was chosen as the reference image. For the rest of the images in the set of five, only the central "keyhole" of *k*-space data was used, and the higher-order *k*-space terms were supplied from (i.e., shared with) the reference acquisition.
- Zero-padding—for all images, only central *k*-space was used and the higher-order *k*-space terms were filled with zeroes.

Thus, the difference between these analyses was whether the full *k*-space data from each of the acquisitions were included in the reconstruction and analysis (conventional) or whether the high *k*-space terms from most of the acquisitions were not included, being replaced instead by those from the reference image acquisitions (keyhole) or by zero values (zero-padding).

The MRI experiments were performed on a 1.5 T Siemens VISION whole-body MR system (Erlangen, Germany) using a circularly polarized head coil. The system has a gradient capability of 25 mT/m with a ramp time of 1.2 ms. To limit subject motion artifacts, a soft cushion was used to keep the head of the volunteer still and comfortable.

Six healthy right-handed male volunteers (ages 27–41 years) participated in the fMRI studies, each of whom had given their informed consent. A 2D fast low-angle shot (FLASH) sequence was used, with the following imaging parameters: $TR/TE/\theta$ = 84 ms/60 ms/25°; slice thickness, 3–4 mm; field of view (FOV), 256 mm, and matrix size 256 × 256. The sequence had first-order flow compensation in all three imaging directions. A reduced bandwidth of 49 Hz/pixel was used to gain a high SNR. At the beginning of each volunteer session, map shimming was conducted with a gradient offset tolerance of 0.0006 mT/m.

For the activation state, volunteers touched each of the fingertips of their dominant hand to the thumb consecutively. For the resting state, volunteers were instructed to simply remain relaxed. To locate the optimal slice position, trial functional studies were performed using the above 2D FLASH sequence with multiple sequential paratransverse slices covering the motor cortex area. Then, three cycles of finger-tapping off-on studies were conducted along the predetermined optimal slice position, with each off-on cycle consisting of five sequentially collected resting state images followed by five sequential activation state images.

Data analysis was performed on images reconstructed by conventional full *k*-space, keyhole, and zero-padding methods. For each subject, three different amounts of

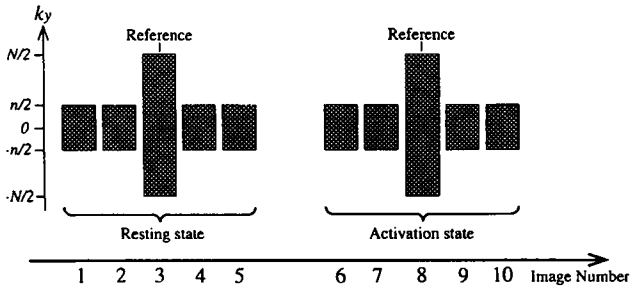

FIG. 1. An example of the keyhole fMRI data acquisition strategy. In this case, five raw *k*-space data sets were collected for each state (resting and activation). For each state, the middle image is chosen as a reference image for that state. *N* and *n* are the total phase-encoding steps for full *k*-space (reference) and keyhole data acquisition strategies, respectively.

data sharing were performed for the keyhole approach, using central 128-, 64-, or 32 *k*-space lines, respectively. These will be referred to as K-128, K-64, and K-32. The corresponding zero-padding reconstruction will be denoted by Z-128, Z-64, and Z-32. Thus, each of these image acquisitions would have taken approximately only one-half, one-quarter, and one-eighth, respectively, of the conventional image acquisition time per image. For the keyhole analysis, the image acquisition data from the middle sample of each series of five were used as the reference images for that set of five. The peripheral lines from the reference image *k*-space data were combined with the central *k*-space data for each of the other images in that half-cycle. Therefore, six reference images (three for the resting state and three for the activation state) were used in our fMRI keyhole analysis for these three-cycle experiments.

In the first step, a pixel-by-pixel group *t*-test was performed to analyze the fMRI images. A statistical parametric image (SPI) of the *t*-statistic distribution was constructed for each different data analysis method (i.e., conventional full *k*-space, keyhole, and zero-padding).

Repeatedly using the same set of high-order phase-encoded lines from a single reference image to complete *k*-space for each keyhole acquisition image in that half-cycle (i.e., resting or activation state) unavoidably introduces a data correlation for each group. The degree of data correlation will increase as more high-order phase-encoded lines are shared for each group. The viability of the group t-test is based on the assumption that each datum is independently sampled, such that the noise across the samples is uncorrelated. Thus, the partial data correlation resulting from data sharing in the keyhole and zero-padding (sharing zero) approaches should be considered in generating the SPI. For conventional full *k*-space data analysis, the effective sampling size (number of independent images) is equal to the total number of the images acquired. For the keyhole and zero-padding analyses, an appropriate adjustment of the effective sampling size to account for the partial correlation can be estimated by calculating the full width at half maximum (FWHM) of the temporal autocorrelation function. To determine the FWHM, we used the standard method of first calculating for each pixel the variance of the derivative of that pixel's values across the series of images and then averaging these variances across all pixels (12–14). The effective sampling size, which is used to calculate the t value for every pixel, for each different analysis, was calculated by dividing the total number of the acquired images by their corresponding values of FWHM. The calculated effective sampling size for the different analyses is shown in Table 1. The SPI was then t thresholded, such that any pixel with a t value greater than a threshold value (t = 2.4) was kept. Any pixel with a t value less than threshold was assigned a value of zero.

For enhancing the sensitivity and specificity of the detection of brain activation, further analysis of the t-thresholded SPI was performed by using a clustered-pixels analysis method (13). In this method, the spatial extent of brain activations is taken into account in addition to the t-value threshold in assessing the significance level. A spatial extent threshold (specified cluster size), K, is determined, which is a function of the threshold t, the significance level ($P = 0.01$ used in this study), the area of the searched brain region (9200 pixels used in this study), and the effective spatial resolution. The effective spatial resolution was estimated by computing the FWHM of the *spatial* autocorrelation function for each conventional, keyhole, and zero-padding analysis (13, 14). The results, along with the value of extent-threshold K determined in each reconstruction technique (full *k*-space, keyhole, and zero-padding), are summarized in Table 1. The results clearly show that the effective spatial resolution in the keyhole approach remained unchanged compared with the original image. However, the effective spatial resolution in the zero-padding approach was significantly degraded. Consequently, it is expected that zero-padding also results in a corresponding weakening of the signal change because of partial volume effects.

The final stage is to apply the extent threshold to the t-thresholded SPI. The extent-threshold value (K) is generally different for the different data analyses (Table 1). Only pixel clusters larger than or equal to K are considered as a real fMRI signal, and any cluster with a size less than K is considered to be noise and is eliminated in the final image. The significant functional activation map ($P < 0.01$: combination of t and spatial extent threshold) was displayed in color scale and superimposed onto a gray-scale anatomic image.

RESULTS

The comparison among the conventional, keyhole, and zero-padding techniques revealed that all three approaches found strong signal changes in the motor cortex during the active finger-tapping task for each of the six subjects.

Table 1
The effective sampling size, effective spatial resolution, t threshold, and extent threshold of the full *k*-space, keyhole, and zero-padding analyses

	Conventional full *k*-space	Keyhole method			Zero-padding method		
		K-128	K-64	K-32	Z-128	Z-64	Z-32
Effective sampling size	30	26	22	19	30	30	30
Effective pixel size (mm)	1.1 ± 0.1	1.1 ± 0.1	1.1 ± 0.1	1.1 ± 0.1	1.4 ± 0.1	2.0 ± 0.2	2.7 ± 0.2
t threshold	2.4	2.4	2.4	2.4	2.4	2.4	2.4
extent threshold	5	6	7	8	7	11	18

The activation map generated by a combination of t and extent thresholds will have a significance of $P < 0.01$.

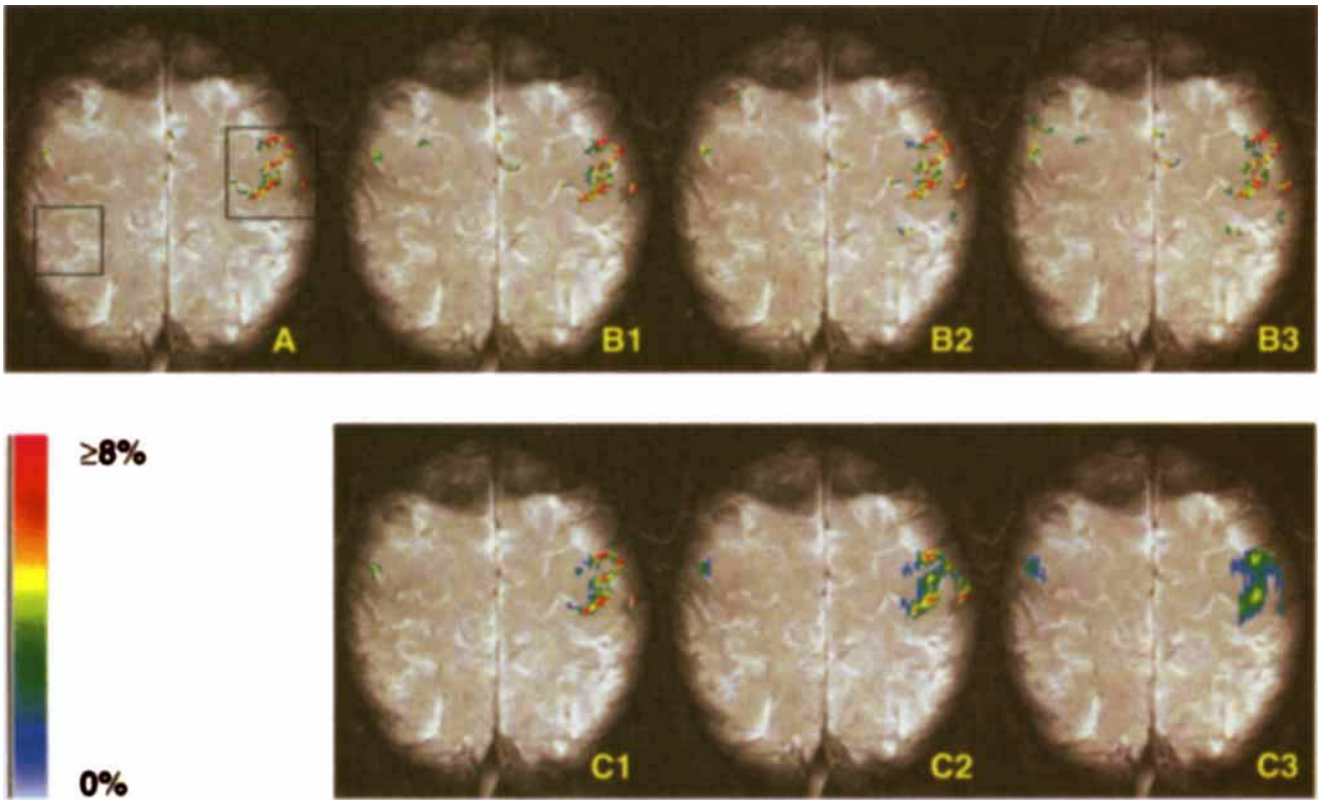

FIG. 2. Functional MR images of subject 1 during the finger-tapping task ($P < 0.01$). (A) An fMRI image obtained from the conventional full *k*-space analysis; the significantly activated area (obtained as described in the Methods section) is superimposed in color onto the anatomic image. The color scale corresponds to the percentage of signal change in the finger-tapping task relative to the rest condition. (B1, B2, B3) show fMRI images derived with the keyhole analysis using 128, 64, and 32 lines of central *k*-space, respectively. (C1, C2, C3) show fMRI images derived with the zero-padding analysis using 128, 64, and 32 lines of central *k*-space, respectively.

Table 2
The activation areas (unit in mm^2) within the motor cortex for the finger-tapping task using conventional full *k*-space, keyhole, and zero-padding analyses

Subject	Conventional full *k*-space	Keyhole method			Zero-padding method		
		K-128	K-64	K-32	Z-128	Z-64	Z-32
1	125	153	179	200	191	270	327
2	34	28	35	56	44	91	167
3	48	46	51	51	68	97	141
4	148	134	153	168	254	317	404
5	39	38	44	42	56	83	136
6	81	90	101	109	126	219	342

Table 3
Mean activation intensity (average of percent intensity signal change) in the activation area within the motor cortex for the finger-tapping task using conventional full *k*-space, keyhole, and zero-padding analyses

Subject	Conventional full *k*-space	Keyhole method			Zero-padding method		
		k-128	k-64	k-32	z-128	z-64	z-32
1	4.86	4.51	4.37	4.25	3.81	3.04	2.34
2	11.72	10.58	11.31	11.65	10.08	7.55	6.73
3	21.04	22.45	20.28	17.88	15.93	10.50	7.55
4	18.28	19.59	18.33	17.36	14.17	11.04	8.46
5	19.15	20.02	18.71	18.09	14.84	10.46	7.06
6	14.34	14.64	14.30	13.83	12.99	10.53	7.15

Figure 2 shows the functional images obtained from the conventional, keyhole, and zero-padding analyses for a typical subject (subject 1, see Tables 2 and 3). The fMRI images obtained from the other five subjects showed a similar pattern. In Fig. 2A, where for the finger-tapping task significant activation areas from the conventional full *k*-space analysis are superimposed in color onto the anatomic image, clear activations of the motor cortex can be seen. The color represents the percentage of changes in signal intensity in the finger-tapping task relative to the rest condition. Figures 2B1, 2B2, and 2B3 show the analogous images of significant activation obtained from the keyhole K-128, K-64, and K-32 approaches, respectively. These images show that the major features of the brain activation—location and intensity—are similar for both the conventional and keyhole analyses. Figures 2C1, 2C2, and 2C3 show the analogous images of significant activation obtained from the zero-padding Z-128, Z-64, and Z-32 approaches, respectively. The fMRI image produced from the zero-padding analysis shows the brain activation area to be substantially larger, and the intensity significantly weaker, than in the image produced from the conventional analysis.

To compare the conventional, keyhole, and zero-padding techniques, it is also necessary to examine the variability of the measured signal intensity across the time course of the experiment. Figure 3 demonstrates the activation time course for a typical subject (subject 1) for the conventional, keyhole, and zero-padding analyses (from the same data session). Figure 3A shows the average signal intensity for the activation area within the motor cortex (colored pixels within the box on the extreme right in Fig. 2A), for the conventional analysis during the cycling of resting-state and finger-tapping conditions. Correspondingly, Figs. 3B1, 3B2, and 3B3 show the time course of the average signal intensity for the activation area within the motor cortex for the keyhole K-128, K-64, and K-32 analysis, respectively. Figures 3C1, 3C2, and 3C3 show the time course of the average signal intensity for the activation area within the motor cortex for the zero-padding Z-128, Z-64, and Z-32 analyses, respectively. Note the strong similarity in the time course and in the spread of data values for the keyhole and conventional analyses, which is consistent with the view that the keyhole analysis captures the salient signal changes effectively. However, the signal change was considerably smaller in the zero-padding analysis compared with the conventional whole *k*-space analysis. The results are consistent with the argument that the enlarged effective pixel size in the zero-padding treatment will increase partial volume effects and will result in a smaller signal change. We also observed a "control" time course of signal intensity for an area in nonmotor cortex (pixels within the box on the extreme left in Fig. 2A) and found no significant change during the resting-state and finger-tapping task conditions (Fig. 3A1). The relatively flat pattern shown in Fig. 3A1 also demonstrates that no apparent system instability exists.

The mean activation area and intensity in the motor cortex for the finger-tapping task for each subject are detailed in Tables 2 and 3, respectively. Based on the data shown in Tables 2 and 3, we calculated the average deviation (percentage difference) in both activation intensity and area being derived from the data-sharing analyses (keyhole and zero-padding) relative to the activation derived from the conventional full *k*-space analysis. Figures 4 and 5 show that the fMRI images produced from the keyhole analysis are closer in intensity and extent to the original ones generated by the conventional whole *k*-space analysis than they are to the zero-padding analysis. In general, the smaller the amount of data sharing, the smaller the difference is. For K-128 analysis, there is no significant difference for fMRI images compared with the original ones. For the K-64 and K-32 analyses, we observed only a modest change in activation intensity and area compared with the original ones (area increases of 16 and 31%, respectively, and intensity decreases of 3 and 7%, respectively). However, for the zero-padding analysis, the differences relative to full *k*-space analysis ranged from 49% (Z-128 analysis) to

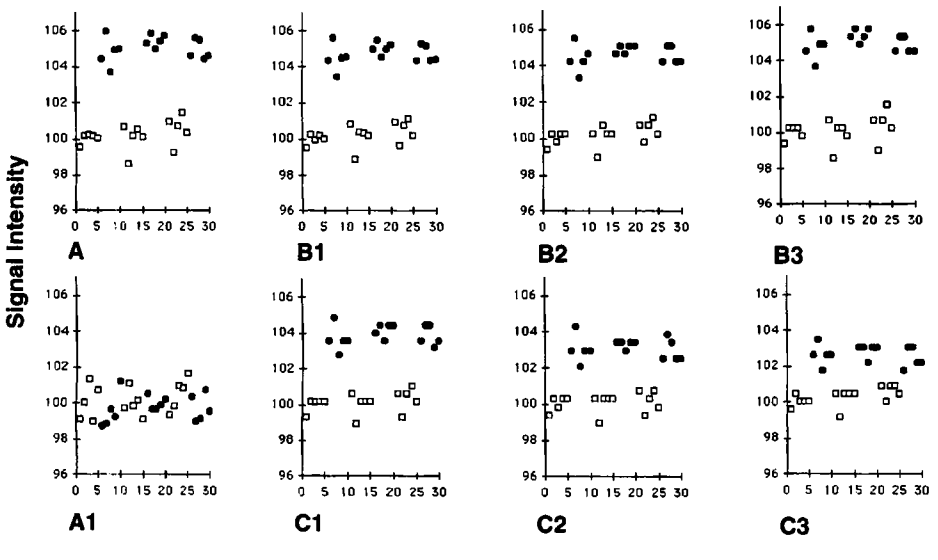

FIG. 3. Time course of the signal-intensity changes in subject 1 for the activation area within the motor cortex during the resting state (open squares) and during the finger-tapping task (dark circles). (A) Conventional full *k*-space analysis; (A1) nonmotor area central analysis; (B1, B2, B3) keyhole analysis using 128, 64, and 32 lines of central *k*-space, respectively; (C1, C2, C3) zero-padding analyses using 128, 64, and 32 lines of central *k*-space, respectively.

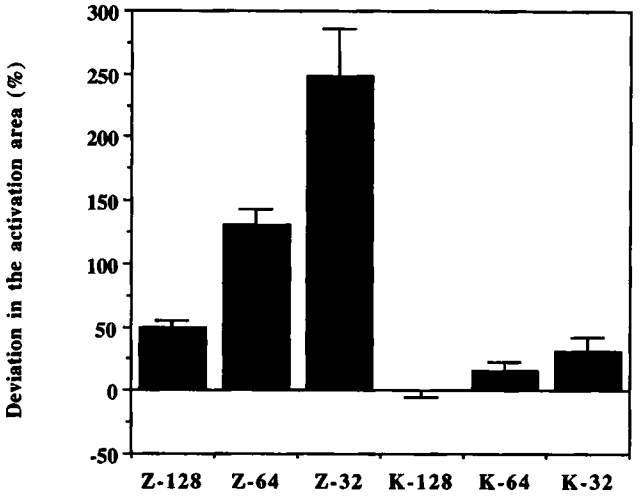

FIG. 4. The mean deviation in the activation area using the keyhole and zero-padding analysis compared with the conventional full *k*-space analysis. K-128, K-64, and K-32 correspond to the keyhole approach using the central 128, 64, and 32 lines of *k*-space, respectively. Z-128, Z-64, and Z-32 correspond to the zero-padding approach using the central 128, 64, and 32 lines of *k*-space, respectively. [The deviation in the activation area = (the activation area generated from the data-sharing analysis minus the activation area generated from the conventional analysis), divided by the activation area generated from the conventional analysis.]

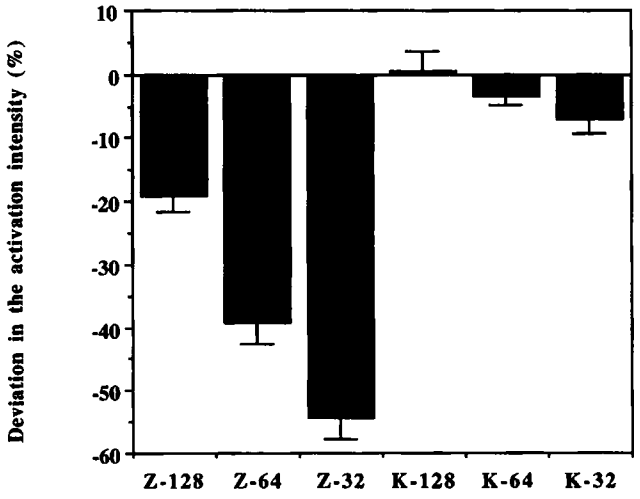

FIG. 5. The mean deviation in the intensity within the activation area using the keyhole and zero-padding analysis compared with the conventional full *k*-space analysis for six subjects. K-128, K-64, and K-32 correspond to the keyhole approach using the central 128, 64, and 32 lines of *k*-space, respectively. Z-128, Z-64, and Z-32 correspond to the zero-padding approach using the central 128, 64, and 32 lines of *k*-space, respectively. [The deviation in the activation intensity = (the activation intensity generated from the data-sharing analysis minus the activation intensity generated from the conventional analysis), divided by the activation intensity generated from the conventional analysis.]

248% (Z-32) area change; and the intensity differences ranged from 19% (Z-128 analysis) to 54% (Z-32). Overall, the analysis clearly demonstrates that the keyhole technique has a significant advantage over the zero-padding technique in keeping the original features (both in activation location and intensity) of the high spatial resolution fMRI images.

DISCUSSION AND CONCLUSIONS

The present study demonstrates that the keyhole gradient-echo technique can be applied to fMRI studies with a significant improvement in temporal resolution and with the major features of the fMRI signal preserved. In this study, we demonstrated that the time savings for achieving high spatial resolution fMRI images using the keyhole technique can be up to a factor of 8. The most economical advantage of this keyhole technique is based on the fact that its data acquisition can be implemented in a conventional MRI system without expensive hardware upgrading. The keyhole fMRI images eventually achieved spatial resolution that was nearly identical to that of the original fMRI images derived by the conventional full *k*-space analysis (Table 1). That our functional MRI keyhole images show no significant spatial distortion is consistent with the results previously obtained by others in (nonfunctional) keyhole imaging (15).

Although our initial effort was in applying the keyhole technique to conventional gradient-echo fMRI images, in principle, the keyhole method can also be extended to other fMRI data acquisition strategies, such as the fast spin-echo and 3D techniques (16–19). Further extending the keyhole method to EPI data acquisition may allow attaining temporal resolution of fMRI in tens of milliseconds, which would provide extraordinarily rapid acquisition of functional brain activation data.

Comparisons were also made with the zero-padding approach. Our study indicated that the zero-padding analysis will produce significant deviations in activation relative to the truly high-resolution fMRI images (conventional full *k*-space analysis). These deviations include substantially degraded spatial resolution and diluted activation-change amplitudes (Figs. 2–5; Table 1). Thus, the zero-padding technique should by no means be considered a good method for achieving high spatial resolution fMRI.

Because of limited *k*-space sampling, the keyhole technique has the potential for artifacts resulting from amplitude and phase discontinuities at the junction of the dynamic low *k*-space data and reference high *k*-space data (20–22). In our current keyhole fMRI studies, there did not appear to be significant image artifacts. The solution for investigators who have encountered image artifacts associated with this discontinuity is to use more sophisticated reconstruction algorithms (21, 22) to remove or minimize image artifacts.

Whereas the significant difference in the zero-padding fMRI images compared with the conventional full *k*-space fMRI images primarily is caused by partial volume effects, we do not yet fully understand the cause of the minimal changes in fMRI images observed in the K-64 and K-32 analysis compared with the conventional full *k*-space analysis. Presumably, these effects relate to some ramifications of the correlations caused by data sharing. Further studies of the SNR behavior of the imaging data in the keyhole analysis and optimization of our statistical method will lead us in determining the underlying prin-

ciples of these observed differences. Regardless, however, these differences appear to be minor relative to the dramatic time savings that can be attained with this technique.

In our study, both t and spatial extent (K) thresholds were used in generating fMRI images. There are many combinations of t and K that satisfy a given significance level p. In this current study, for a given p, we chose a value for t and then determined K. Alternative methods, such as fixing K and then determining t, may affect the appearance of the final fMRI images. A standard procedure should be developed in the data analysis for comparing fMRI images obtained from different laboratories.

In summary, the keyhole technique is an efficient method that can dramatically improve the temporal resolution of dynamic high spatial resolution fMRI images. The time-saving feature of this sequence will, in turn, enable acquiring multiple slices within an acceptable total imaging time. This represents an important advantage for fMRI studies in which multiple slices will generally be preferred to ensure capturing an intended ROI and/or to determine the extent of an activation. Faster acquisition will also provide for more experimental conditions within the same session, a capability that is particularly useful for implementing various cognitive neuroscience paradigms. In addition, the higher time resolution for fMRI achieved by the keyhole technique will allow a more accurate study of the time course of the brain's response to stimulation—an important goal of both basic and clinical neuroscientists.

REFERENCES

1. K. K. Kwong, Functional magnetic resonance imaging with echo planar imaging. *Magn. Reson. Quarterly* **11**, 1–20 (1995).
2. J. J. van Vaals, M. Brummer, W. T. Dixon, H. H. Tuithof, H. Engels, R. C. Nelson, B. M. Gerety, J. L. Chezmar, J. A. den Boer, "Keyhole" method for accelerating imaging of contrast agent uptake. *J. Magn. Reson. Imaging* **3**, 671–675 (1993).
3. R. A. Jones, O. Haraldseth, T. B. Muller, P. A. Rinck, A. N. Oksendal, K-space substitution: a novel dynamic imaging technique. *Magn. Reson. Med.* **29**, 830–834 (1993).
4. J. Bishop, R. M. Henkelman, D. B. Plewes, Dynamic spin-echo imaging: theoretical assessment and implementation. *J. Magn. Reson. Imaging.* **4**, 843–852 (1994).
5. S. J. Riederer, T. Tasciyan, R. Farzaneh, J. N. Lee, R. C. Wright, R. J. Herfkens, MR fluoroscopy: technical feasibility. *Magn. Reson. Med.* **8**, 1–15 (1988).
6. G. B. Pike, J. O. Fredrickson, G. H. Glover, D. R. Enzmann, Dynamic susceptibility contrast imaging using a gradient-echo sequence, *in* "Proc., SMRM, 11th Annual Meeting, Berlin, 1992," p. 1131.
7. R. S. Hinks, S. Einstein, Shared data dual echo in fast spin-echo imaging, *in* "Proc., SMRM, 10th Annual Meeting, San Francisco, 1991," p. 1011.
8. J. E. Bishop, I. Soutar, W. Kucharczyk, D. B. Plewes, Rapid sequential imaging with shared-echo fast spin-echo imaging, *in* "Works in Progress Supplement to Annual Meeting Program, SMRI, 10th Annual Meeting, New York, 1992," p. S22.
9. H. D. Morris, Z.-P. Liang, C. Potter, Y. Cao, P. C. Lauterbur, Efficient functional imaging with RIGR on a clinical system, *in* "Proc., SMRM, 12th Annual Meeting, New York, 1993," p. 1393.
10. J.-H. Gao, J. Xiong, J. Li, M. Woldorff, J. Schiff, P. T. Fox, Dynamic functional NMR imaging studies using conventional MRI systems, *in* "Proc., ENC, 36th Annual Meeting, Boston, MA, 1995," p. 248.
11. J. Tintera, G. Schaub, J. Gawehn, P. Stoeter, Functional MRI with keyhole technique, *Human Brain Mapping*, supplement 1, 124 (1995).
12. K. J. Friston, P. Jezzard, R. Turner, Analysis of functional MRI time-series. *Human Brain Mapping* **1**, 153–171 (1994).
13. J. Xiong, J.-H. Gao, J. Lancaster, P. T. Fox, Clustered pixels analysis for functional MRI activation studies of the human brain. *Human Brain Mapping* **3** (4), (1995).
14. K. J. Worsley, A. C. Evans, S. Marrett, P. Neelin, A three-dimensional statistical analysis for CBF activation studies in human brain. *J. Cereb. Blood Flow Metab.* **12**, 900–918 (1992).
15. T. A. Spraggins, Spatial distortions in keyhole imaging, *in* "Proc., SMRM, 12th Annual Meeting, New York, 1993," p. 1259.
16. R. T. Constable, R. P. Kennan, A. Puce, G. McCarthy, J. C. Gore, Functional NMR imaging using fast spin echo at 1.5 T. *Magn. Reson. Med.* **31**, 686–690 (1994).
17. J.-H. Gao, J. Xiong, J. Li, J. Schiff, J. Roby, J. Lancaster, P. T. Fox, Fast spin-echo characteristics of visual stimulation-induced signal changes in the human brain. *J. Magn. Reson. Imaging* **5**, 709–714 (1995).
18. P. V. Gelderen, N. F. Ramsey, G. Liu, J. H. Duyn, J. A. Frank, D. R. Weinberger, C. T. Moonen, Three dimensional functional magnetic resonance imaging of human brain on a clinical 1.5-T scanner. *Proc. Natl. Acad. Sci. (USA)* **92**, 6906–6910 (1995).
19. E. M. Haacke, A. Hopkins, S. Lai, P. Buckley, L. Friedman, H. Meltzer, P. Hedera, R. Friedland, S. Klein, L. Thompson, D. Detterman, J. Tkach, J. S. Lewin, 2D and 3D high resolution gradient echo functional imaging of the brain: venous contributions to signal in motor cortex studies. *NMR Biomed.* **7**, 54–62 (1994).
20. X. Hu, On the "keyhole" technique, *J. Magn. Reson. Imaging* **4**, 231 (1994).
21. Z. P. Liang, P. C. Lauterbur, Improved temporal/spatial resolution in functional imaging through generalized series reconstruction, *in* "Works in Progress Supplement to Annual Meeting Program, SMRI, 10th Annual Meeting, New York, 1992," p. S15.
22. Z. P. Liang, P. C. Lauterbur, Efficient time-sequential imaging through generalized series modeling: a simulation analysis, *in* "Proc., SMRM, 11th Annual Meeting, Berlin, 1992," p. 4266.